IEEE Access
Multidisciplinary ⋮ Rapid Review ⋮ Open Access Journal

Received April 25, 2020, accepted May 5, 2020, date of publication May 20, 2020, date of current version June 16, 2020.

Digital Object Identifier 10.1109/ACCESS.2020.2994437

Investigation of Intelligent Vehicle Path Tracking Based on Longitudinal and Lateral Coordinated Control

ZEYU SUN, RUOCHEN WANG, QING YE, ZHENDONG WEI, AND BINGQING YAN
School of Automotive and Traffic Engineering, Jiangsu University, Zhenjiang 212013, China

Corresponding author: Ruochen Wang (wrc@ujs.edu.cn)

This work was supported by the Synergistic Innovation Center of Jiangsu Modern Agricultural Equipment and Technology, China, under Project 4091600031.

ABSTRACT In this paper, a new longitudinal and lateral coordinated control algorithm for the intelligent vehicle (IV) is proposed for the problem of unbalance of tracking accuracy and vehicle stability during path tracking process. This work proposes a novel algorithm that adopts hierarchical control architecture and local linearization of the nonlinear path tracking model, establishes the objective function by tracking performance and driving performance in the tracking process, and designs the upper optimal controller. Following the theory of fuzzy proportional–derivative control method, a low-speed tracking controller is designed to track the desired speed. Simulations and the hardware-in-the-loop test are utilized to verify the effectiveness of the designed path tracking control algorithm. Results show that, unlike the traditional fixed-speed tracking control method, the proposed vertical and horizontal coordinated control algorithm can guarantee the vehicle's tracking performance at different speeds and improve its form stability. The improved effect is evident even at high speed.

INDEX TERMS Intelligent vehicle, path tracking, layered, longitudinal and lateral coordinated control.

I. INTRODUCTION

Intelligent vehicle motion control includes lateral, longitudinal, and vertical and horizontal coordinated motion control. Lateral motion control is the steering control of the vehicle. Longitudinal control is the control of the longitudinal displacement, vehicle speed, and acceleration of the vehicle. Vertical and horizontal coordinated control is the tracking of the desired path and state through the comprehensive control of the vertical and horizontal systems of the vehicle [1].

Lateral control, as the basis of intelligent vehicle path tracking control, has been extensively studied [2]–[8]. Following proportional–integral–derivative (PID) control theory, Marino *et al.* [9] designed a nested PID lateral controller to offset the impact of uncertain road curvature on path tracking stability. Goodarzi *et al.* [10] used the curvature of the road and the tracking error of the vehicle as the feedforward and feedback signals of the controller, respectively, and controlled the optimal front wheel steering and yaw moment required for real-time tracking through a linear quadratic regulator. Tomizuka *et al.* [11] studied the special working conditions of a smart car's rear wheel sensor failure, and they used the state feedback linear method to design the lateral controller and assumed that the control system is a linear time-varying system. Duan *et al.* [12] proposed an effective path tracking control algorithm with speed adjustment, which used an improved PID controller for tight path tracking, and suggest a feed-forward control method to eliminate the heading errors caused by dynamic conditions while tracking a desired path. Gámez Serna and Ruichek [13] considered road curvature with speed limits and used Dynamic Speed Adaptation method to adjust vehicle's speed.

Intelligent vehicle longitudinal control is based on the acquisition of vehicle and road information, and the coordinated control of the drive/brake enables the vehicle to track the desired vehicle speed stably [14]. HosseinNia *et al.* [15] proposed an optimized fractional order control method for autonomous vehicles in low-speed driving during a traffic jam and designed two different PI controllers following PID control theory to control the throttle and brake of vehicles and ultimately ensure the safety performance of vehicles during traffic jams. Maojing [16] used the curvature of the road as

The associate editor coordinating the review of this manuscript and approving it for publication was Atif Iqbal.

the influence factor of the expected acceleration and designed the brake controller on the basis of the terminal sliding mode control algorithm. The simulation results showed that the controller can stably track the expected acceleration and reduce the influence of road curvature and other disturbances effectively with good robustness. To achieve vehicle energy saving and improve ride comfort, Fang *et al.* [17] proposed a novel intelligent vehicle longitudinal motion control by stratified optimization method. The upper controller works according to the Radau pseudo-spectrum method, and the lower controller is model predictive control. Ultimately, it can effectively reduce the running energy while accurately tracking the target trajectory. Majdoub *et al.* [18] studied the modeling problem of longitudinal motion of front-wheel-drive vehicles and developed a smart car longitudinal nonlinear controller through Lyapunov design, effectively realizing the precise adjustment of the chassis and wheel speed.

The actual path tracking process of the vehicle is completed by the coordination between the vertical and horizontal motion systems, which have a complex coupling relationship. Single-direction motion control cannot achieve accurate path tracking of the vehicle [19], [20]. Li *et al.* [21] investigates the optimal model predictive control for the path tracking of an autonomous vehicle, and take the path tracking error and the energy consumed into consideration. Menhour *et al.* [22] proposed a model-free control scheme and used it in a multivariable decoupling vertical and horizontal control system by adjusting the driving/braking torque and angle. The simulation results showed that the control scheme has good robustness to model error and parameter uncertainty of vertical and horizontal coupling. Duan *et al.* [12] proposed an effective path tracking control algorithm with speed adjustment, and also taking consideration of dynamic restrains, besides, they use an improved circle look-ahead (CLA) with a PID controller for tight path tracking, and suggest a feed-forward control method to eliminate the heading errors caused by dynamic conditions while tracking a desired path. On the basis of the nonlinear three-degrees-of-freedom passenger car dynamics model, Kumarawadu and Lee [23] coordinated the control of a vehicle's horizontal and vertical systems by combining the proportional–derivative (PD) algorithm with the neural network adaptive algorithm.

In summary, the current performance evaluation index of the path tracking controller is limited to tracking accuracy and robustness, and the vehicle handling stability evaluation index is not included in the path tracking system. The stability of the vehicle can easily deteriorate through a single front wheel angle control under high-speed driving conditions, and the coupling relationship between the vehicle tracking control accuracy and the vehicle running stability cannot be effectively coordinated. Thus, on the basis of the hierarchical control idea, we design a hierarchical path tracking control system in which the upper controller follows optimal control theory and the lower controller tracks the expected vehicle speed based on the fuzzy PD control theory. For this design, we take the tracking performance and driving performance of the vehicle as indicators to plan the current optimal front wheel angle and optimal vehicle speed in real time. Then, a fuzzy corner compensation controller is designed for the nonlinear part of the model. The actual longitudinal vehicle speed outputted by the CarSim vehicle module in the closed-loop simulation is taken as the coupling point. The vehicle control system is composed as the input of the optimal controller. The joint simulation of CarSim and Simulink is conducted to verify the performance of the designed path tracking controller. The hardware-in-the-loop (HIL) test verifies that the designed vertical and horizontal control system can improve the driving stability of the vehicle without affecting the tracking accuracy.

The innovation of the paper is mainly as follow: 1) A hierarchical control algorithm is proposed on the basis of the hierarchical control theory and fuzzy PD control theory to improve the intelligent vehicle path tracking accuracy and robustness, 2) The coupling mechanism of IV longitudinal and lateral motion is considered, and the vehicle handling stability, tracking accuracy and robustness evaluation index are considered in the controller designed.

The rest of this paper is organized as follows: Section 2 establishes a path tracking system model including vehicle dynamics model, vehicle power transmission model and preview error model; Section 3 proposes a hierarchical path tracking controller of intelligent vehicle based on the optimal control theory and fuzzy PD control theory; Section 4 validates the effectiveness and superiority of the proposed hierarchical path tracking control method in path tracking and handling performance improving through simulation analysis; Section 5 carries out a bench test which verifies the correctness of the simulation results; Section 6 presents the general conclusion.

II. PATH TRACKING SYSTEM MODEL

The path tracking system model is the basis of intelligent vehicle path tracking. To perform closed-loop simulation of the path tracking system, three relevant dynamic models, namely, vehicle dynamics model, vehicle transmission model, and visual error model, are constructed. These models are shown in Fig 1.

A. VEHICLE DYNAMICS MODEL

To reflect the kinematics and dynamics of the vehicle path tracking process accurately and to consider the simplicity of the model, the following are initially assumed: 1) the road is flat enough, that is, the vertical movement of the vehicle is disregarded; 2) the role of the suspension system is ignored; 3) the steering angle directly acts on the front wheels of the vehicle, and the angles of the left and right wheels are equal; and 4) all the sub-components in the vehicle dynamic transmission system can achieve the ideal transmission efficiency.

The vehicle model with three degrees of freedom is shown in Fig 2.

In accordance with the dynamics of the vehicle's longitudinal, lateral, and yaw directions and Newton's law of motion,

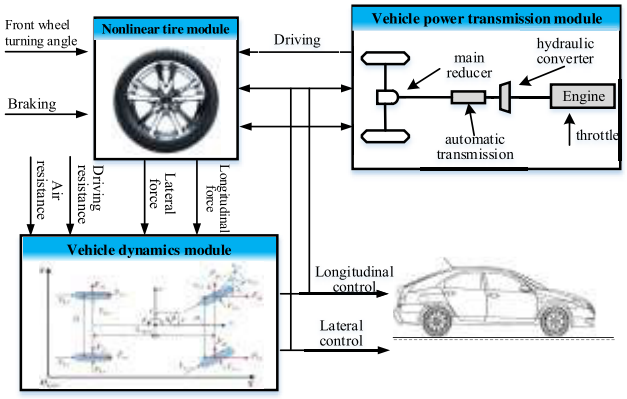

(a)

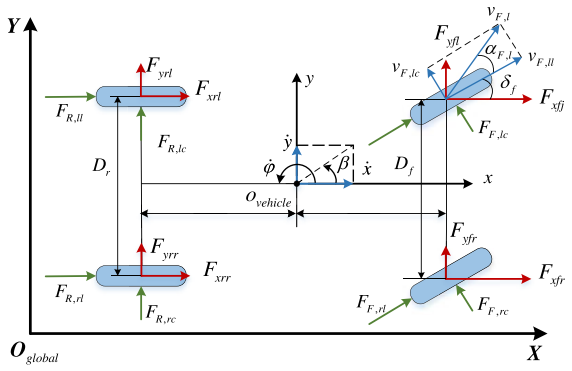

(b)

FIGURE 1. Structure diagram of path tracking system. (a) Path tracking system model; (b) Vehicle dynamics model.

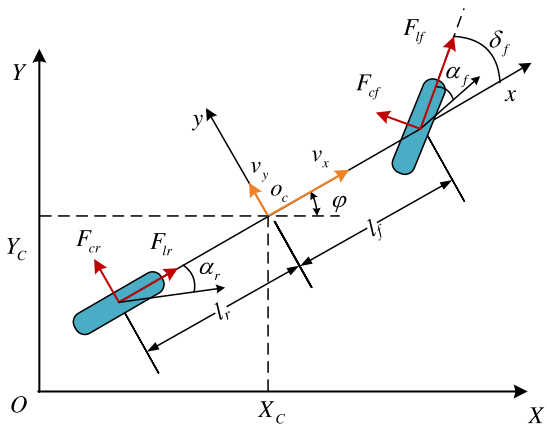

FIGURE 2. Three-degree-of-freedom monorail vehicle model.

the vehicle dynamics model can be expressed as follows:

$$\begin{cases} m\dot{v}_x = ma_x = mv_y\dot{\varphi} + 2C_{\lambda f}\lambda_f + 2C_{\lambda r}\lambda_r \\ m\dot{v}_y = -mv_x\dot{\varphi} + 2C_{\alpha f}\left(\delta - \dfrac{v_y + l_f\dot{\varphi}}{v_x}\right) - \dfrac{2C_{\alpha r}\left(v_y - l_r\dot{\varphi}\right)}{v_x} \\ I_Z\ddot{\varphi} = 2l_f C_{af}\left(\delta_f - \dfrac{v_y + l_f\dot{\varphi}}{v_x}\right) + \dfrac{2l_r C_{\alpha r}\left(v_y - l_r\dot{\varphi}\right)}{v_x} \end{cases} \tag{1}$$

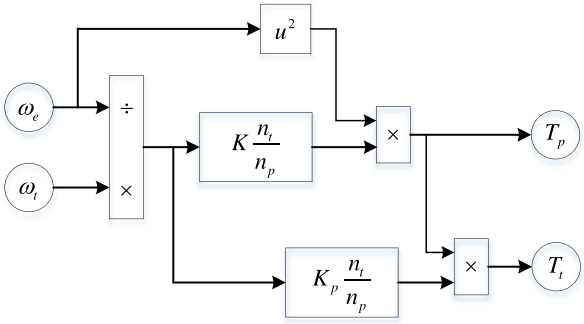

FIGURE 3. Characteristic schematic diagram of hydraulic torque converter.

where a_x is the longitudinal acceleration; r is the yaw rate; m is the vehicle mass; δ_f is the front wheel angle; I_z is the vehicle's moment of inertia around the axis Z; I_f and I_r are the front and rear wheelbase of the vehicle, respectively; v_x and v_y are the longitudinal and transverse speeds, respectively; and C_{af} and C_{ar} are the lateral stiffness of the front and rear tires, respectively.

B. POWER TRANSMISSION MODEL AND TIRE MODEL OF THE VEHICLE

During the actual vehicle operation, the nonlinear disturbance of the whole vehicle transmission system interferes with the longitudinal motion control accuracy and robustness. Such interference is primarily due to the driving force, driving resistance, and braking force acting on the front and rear wheels. Therefore, on the basis of block modeling, we establish a longitudinal power train model, which includes the engine, torque converter, automatic transmission, and final drive.

1) ENGINE MODEL

Taking a four-stroke fuel-injected gasoline engine as an example [24], the relationship between the steady-state output torque of the engine T_e and the engine speed ω_e and throttle opening α can be described as:

$$T_e = f_e\left(\omega_e, \alpha\right) \tag{2}$$

where f_e is the non-linear function of the steady-state torque characteristic of the engine.

Given the hysteresis in the operation of engine, a first-order inertia link is introduced in the above engine steady-state model to describe this inertial property, namely,

$$f_e\left(\omega_e, \alpha\right) = T_e + T_1\dot{T}_e \tag{3}$$

where T_1 is the first order inertia constant.

2) HYDRAULIC TORQUE CONVERTER MODEL

The torque converter is the connecting part of the engine and the drive train. It is composed of a pump wheel, a turbine, and a working fluid. The torque is transmitted from the pump wheel to the turbine through hydrokinetic transmission. Li

TABLE 1. Ratio of automatic transmission.

Gears	Transmission ratio	Gears	Transmission ratio
1	2.91	3	1
2	1.59	4	0.69

[?] gives the principle diagram of the torque converter which shows in Fig. 3.

The relationship between the available turbine output torque and the pump input speed is

$$T_t = K \cdot K_p \frac{n_t^2}{n_p^2} n_p^2 \tag{4}$$

where n_t is the turbine speed; n_p is the pump wheel speed; T_t is the turbine torque; K is the capacity factor; K_p is the torque characteristic coefficient.

3) AUTOMATIC TRANSMISSION MODEL

We take the four-speed planetary gear-type automatic transmission as the research object, and its specific transmission is shown in Table 1.

The automatic transmission can automatically shift and adjust the torque during the running of the vehicle. The output speed and torque can be expressed as

$$\begin{cases} n_d = n_t / r_g \\ T_d = T_t \cdot r_g \end{cases} \tag{5}$$

where n_d is the output speed of the automatic transmission, T_d is the output torque of the automatic transmission, and r_g is the transmission ratio.

4) MAIN REDUCTION GEAR MODEL

We choose a bevel gear main reducer with a transmission ratio of $r_0 = 2.87$.

C. PREVIEW ERROR MODEL

Vehicle path tracking control system can be divided into two types according to vehicle sensors: preview and non-preview [25]. Compared with the non-preview control method, the preview control has the advantages of large information and good robustness. To construct the vehicle dynamics model and the transmission model, the vehicle kinematics model is established. We use the traditional visual preview error model, the diagram of which is shown in Fig. 4.

In accordance with the geometric relationship of the above figure, the road following model based on the preview can be expressed as

$$\begin{cases} \dot{y}_e = v_x \varepsilon_e - v_y - \omega_r L \\ \dot{\varepsilon}_e = v_x K_L - \omega_r \end{cases} \tag{6}$$

where y_{ef}, y_{er}, and y_{eo} indicate the lateral deviation of the front and rear axis and center of mass of the vehicle with respect to the pre-point, respectively; y_e is the lateral deviation at the pre-point; and L is the preview distance. K_L is the road curvature.

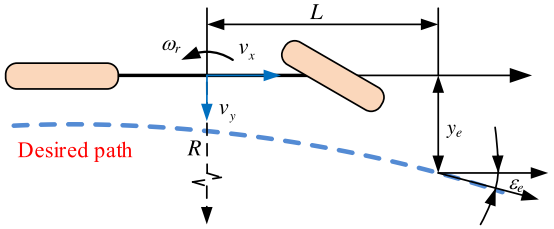

FIGURE 4. Preview error model.

Through the combination of (1) with (6), the vehicle–road dynamics model during vehicle path tracking can be obtained.

$$\begin{cases} \dot{\varphi} = \omega_r \\ \dot{v}_x = a_x \\ \dot{v}_y = A_{11} v_y + A_{12} \omega_r + B_{11} \delta \\ \dot{\omega}_r = A_{21} v_y + A_{22} \omega_r + B_{21} \delta \\ \dot{y}_e = v_x \varepsilon_e - v_y - \omega_r L \\ \dot{\varepsilon}_e = v_x K_L - \omega_r \end{cases} \tag{7}$$

where

$$A_{11} = \frac{-C_{\alpha f} + C_{\alpha r}}{m v_x}; A_{12} = \frac{C_{\alpha r} l_r - C_{\alpha f} l_f}{m v_x} - v_x;$$
$$B_{11} = \frac{C_{\alpha f}}{m}; B_{21} = \frac{C_{\alpha f} l_f}{I_z}; A_{21} = \frac{C_{\alpha r} l_r - C_{\alpha f} l_f}{I_z v_x};$$
$$A_{22} = -\frac{C_{\alpha f} l_f^2 + C_{\alpha r} l_r^2}{I_z v_x};$$

III. PATH TRACKING CONTROL SYSTEM DESIGN

In the actual driving of the vehicle, a constant speed is impossible to maintain while steering due to changes in the path curvature and road conditions. Doing so requires the ability to adjust the speed of the vehicle adaptively, which can be achieved by coordinating the vertical and horizontal systems. Many path tracking control approaches have been presented to handle the tradeoff by the utilization of various control techniques, such as fuzzy control, PID control, neural-network control, optimal control, linear optimal control, adaptive control, and H_∞ control, and their combined methods. In this paper, we propose a hierarchical intelligent vehicle path tracking control system. The control frame diagram is shown in Fig. 5. The upper controller is the optimal controller, whereas the lower controller is the longitudinal speed tracking controller and the lateral corner compensation controller.

A. OPTIMAL CONTROLLER DESIGN

Neither the individual lateral control nor the individual longitudinal control can reflect the driving characteristics of the vehicle's path tracking process. The actual driving situation is

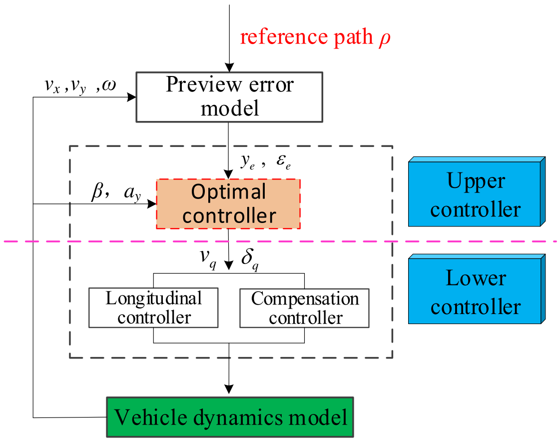

FIGURE 5. Frame of Hierarchical path tracking control system.

generally achieved through the coordinated work of the steering and accelerator/brake pedals. In this section, the upper controller is designed using optimal control algorithm based on the simplified vehicle-road dynamics model.

1) DISCRETIZATION OF PREVIEW TRACKING MODEL

The vehicle–road dynamic model shown by (7) can be expressed by the following nonlinear equation:

$$\dot{x}\,(t) = f\,(x\,(t)\,, u\,(t)) \tag{8}$$

where the state variable is $x\,(t) = \left[v_x, v_y, \varphi, y_e, \varepsilon_e\right]^T$ and the control amount is $u\,(t) = [a_x, \delta]$.

Taylor expansion is performed at the initial state $(x_0\,(t)\,, u_0\,(t))$ with a nonlinear state equation

$$\begin{aligned}\dot{x}\,(t) = f\,(x_0\,(t)\,,\ u_0\,(t-1)) + \frac{\partial f}{\partial x}\left|_{x_0(t),u_0(t-1)}\right.(x\,(t) - x_0\,(t))\\ + \frac{\partial f}{\partial u}\left|_{x_0(t),u_0(t-1)}\right.(u\,(t) - u_0\,(t-1))\end{aligned} \tag{9}$$

where $\frac{\partial f}{\partial x}\left|_{x_0(t),u_0(t-1)}\right.$ and $\frac{\partial f}{\partial u}\left|_{x_0(t),u_0(t-1)}\right.$ represent the Jacobian matrix of the path tracking system with respect to the state quantity x and the control quantity u, respectively.

Subtracting (9) from (8) results in

$$\dot{\hat{x}}\,(t) = A\,(t)\,\hat{x} + B\,(t)\,\hat{u} \tag{10}$$

where

$$A = \begin{bmatrix} \frac{\partial f}{\partial v_x} & \frac{\partial f}{\partial v_y} & \frac{\partial f}{\partial \omega_r} & \frac{\partial f}{\partial y_e} & \frac{\partial f}{\partial \varepsilon_e} \\ \frac{\partial f}{\partial v_x} & \frac{\partial f}{\partial v_y} & \frac{\partial f}{\partial \omega_r} & \frac{\partial f}{\partial y_e} & \frac{\partial f}{\partial \varepsilon_e} \\ \frac{\partial f}{\partial v_x} & \frac{\partial f}{\partial v_y} & \frac{\partial f}{\partial \omega_r} & \frac{\partial f}{\partial y_e} & \frac{\partial f}{\partial \varepsilon_e} \\ \frac{\partial f}{\partial v_x} & \frac{\partial f}{\partial v_y} & \frac{\partial f}{\partial \omega_r} & \frac{\partial f}{\partial y_e} & \frac{\partial f}{\partial \varepsilon_e} \\ \frac{\partial f}{\partial v_x} & \frac{\partial f}{\partial v_y} & \frac{\partial f}{\partial \omega_r} & \frac{\partial f}{\partial y_e} & \frac{\partial f}{\partial \varepsilon_e} \end{bmatrix}$$

$$= \begin{bmatrix} 0 & 0 & 0 & 0 & 0 \\ 0 & \frac{-C_{\alpha f} + C_{\alpha r}}{m v_0} & \frac{C_{\alpha r} l_r - C_{\alpha f} l_f}{m v_0} - v_0 & 0 & 0 \\ 0 & \frac{C_{\alpha r} l_r - C_{\alpha f} l_f}{I_z v_0} & -\frac{C_{\alpha f} l_f^2 + C_{\alpha r} l_r^2}{I_z v_0} & 0 & 0 \\ 0 & -1 & -L & 0 & v_0 \\ K_L & 0 & -1 & 0 & 0 \end{bmatrix};$$

$$B = \begin{bmatrix} \frac{\partial f_1}{\partial a_x} & \frac{\partial f_2}{\partial a_x} & \frac{\partial f_3}{\partial a_x} & \frac{\partial f_4}{\partial a_x} & \frac{\partial f_5}{\partial a_x} \\ \frac{\partial f_1}{\partial \delta} & \frac{\partial f_2}{\partial \delta} & \frac{\partial f_3}{\partial \delta} & \frac{\partial f_4}{\partial \delta} & \frac{\partial f_5}{\partial \delta} \end{bmatrix}^T = \begin{bmatrix} 1 & 0 & 0 & 0 & 0 \\ 0 & \frac{C_{\alpha f}}{m} & \frac{C_{\alpha f} l_f}{I_z} & 0 & 0 \end{bmatrix}^T$$

2) OBJECTIVE FUNCTION SELECTION

The optimal control problem is to find the control function that can achieve the optimum system performance under certain constraints. In other words, optimal control essentially involves finding the optimal control law that enables the specified objective function to reach the extreme value as the controlled system shifts from the initial state to the terminal state. Therefore, choosing the appropriate objective function at the beginning of the optimal controller design is the focus of the controller design.

On the basis of the path tracking control algorithm framework shown in Figs. 1 and 5, we choose the linear quadratic optimal control algorithm as the upper-level algorithm for path tracking control. First, we establish the following objective function:

$$J = \frac{1}{2} X^T F X + \frac{1}{2}\int_{t_0}^{t_f}\left[X^T Q X + U^T R U\right] d_t \tag{11}$$

where F and Q are $n \times n$-order semipositive definite symmetric matrices; R is $r \times r$-order positive definite control weighting matrix; t_0 and t_f are the initial and end moments of the system, respectively. The specific significance of each performance index is as follows:

$\frac{1}{2}\int_{t_0}^{t_f} X^T F X$ is a terminal term that is introduced to limit the size of the terminal error and is characterized as a penalty term for the terminal error. The weighting matrix F indicates the degree of emphasis on the terminal error.

$\frac{1}{2}\int_{t_0}^{t_f} X^T Q X$ is the error integral term, which refers to the sum of the errors of each state quantity from the initial time to the terminal time during the operation of the system. It is characterized as the degree of deviation of the actual operation result from the ideal result. Matrix Q is characterized by the degree of attention the optimal control system attaches to each state vector.

$\frac{1}{2}\int_{t_0}^{t_f} U^T R U$ is the control integral term, which represents the total energy consumed by the controlled system during the entire control process. It is characterized as the control cost paid during the control process. R is characterized as the degree of constraint on the control components of the optimal control system.

To ensure the accuracy of intelligent vehicle path tracking, the tracking error that reflects the tracking performance must be added to the objective function, including the lateral deviation and directional deviation from the look-ahead point.

In addition, to ensure good handling stability during vehicle tracking, the lateral acceleration and sideslip angle of the center of mass are taken as the indicators of vehicle handling stability. In the actual driving of the vehicle during stable tracking of the desired path, when a large road curvature is encountered, only front-wheel steering can easily cause the vehicle to be unstable and even result in a rollover at a high vehicle speed. Therefore, when facing a large road curvature, the vehicle should be able to reduce its speed adaptively. After passing through a large curvature of the road, the vehicle increases its speed to complete fast and stable path tracking.

3) CONSTRAINT ESTABLISHMENT

Based on the established suitable objective function, to ensure the safety factors in the path tracking process, the control amount of the vehicle (the longitudinal acceleration and the front wheel rotation angle) should not exceed a certain threshold. Hence, a certain restriction on the control amount is required.

$$\begin{cases} U_{\min}(k) \le U(k) \le U_{\max}(k) \\ \Delta U_{\min}(k) \le \Delta U(k) \le \Delta U_{\max}(k) \end{cases} \tag{12}$$

where $U_{\min}(k)$ and $U_{\max}(k)$ are the lower and upper limits of the control amount, respectively, which are characterized by the constraints on the longitudinal acceleration and the absolute value of the front wheel rotation angle during the path tracking process; and $\Delta U_{\min}(k)$ and $\Delta U_{\max}(k)$ are the lower and upper limits of the control amount change rate, respectively, which are characterized by the constraints on the longitudinal acceleration and the change rate of the front wheel rotation angle during the path tracking process.

4) WEIGHT MATRIX SELECTION

As mentioned in, Section III.A.2), three weighting matrices F, Q, and R in the objective function are characterized as the constraints of the optimal control system on the terminal error, cumulative error, and control amount during the path tracking process. The intelligent vehicle path tracking process can be regarded as an infinite-time linear quadratic control system. Thus, the influence of terminal errors on the system can be ignored, that is, $F = 0$. The objective function of the path tracking system can be rewritten as

$$J = \int_{t_0}^{\infty} \left(X^T Q X + U^T R U \right) d_t \tag{13}$$

where $X = \left[\dot{v}_y, \beta, y_e, \varepsilon_e\right]^T$; $u(t) = [a_x, \delta]$.

The error term weighting matrix Q and the control variable weighting matrix R are taken as diagonal matrices, respectively.

$$Q = \begin{bmatrix} q_1 & 0 & 0 & 0 \\ 0 & q_2 & 0 & 0 \\ 0 & 0 & q_3 & 0 \\ 0 & 0 & 0 & q_4 \end{bmatrix}, \quad R = \begin{bmatrix} r_1 & 0 \\ 0 & r_2 \end{bmatrix}$$

At a low vehicle speed, the vehicle has good handling performance. At this time, to ensure tracking speed and accuracy, the optimal controller tends to apply small speed changes to meet the tracking accuracy requirements.

At a high vehicle speed, the vehicle has poor handing performance. Therefore, the optimal controller tends to reduce the vehicle speed to ensure good driving performance, that is, improving the handling stability of the vehicle by reducing the acceleration constraints.

When the vehicle speed is in the safe steering range, the optimal controller tends to consider the speed and accuracy of the path being followed. With the fitting tool in MATLAB, the weights of the weighting matrices Q and R are defined as the exponential functions related to the vehicle speed.

5) SOLUTION OF OPTIMAL CONTROL LAW

The objective function and control quantity constraint of the optimal controller are established above, and the weighting matrices Q and R with vehicle speed are selected. The maximum-value principle is applied to solve the above optimal control problem.

The Hamiltonian function H is constructed as

$$H = \frac{1}{2} X^T Q X + \frac{1}{2} U^T R U + \lambda^T \left[AX + BU \right] \tag{14}$$

Following the maximum-value principle, the Hamilton function H should take the maximum value to minimize the performance index function J

$$\frac{\partial H}{\partial U} = RU + B^T \lambda = 0 \tag{15}$$

Then, the optimal control equation is

$$U^* = -R^{-1} B^T \lambda \tag{16}$$

where R and B are known equations. Hence, the solution of the optimal control equation is transformed into the solution of λ.

From the canonical equation, we obtain the following:

$$\dot{X} = \frac{\partial H}{\partial \lambda} = Ax - BR^{-1} B^T \lambda \tag{17}$$

$$\dot{\lambda} = -\frac{\partial H}{\partial X} = -QX - A^T \lambda \tag{18}$$

To achieve linear feedback, λ is generally expressed as a linear function of X about the state vector, that is,

$$\left(\dot{P} + PA - PBR^{-1} B^T P - Q + A^T P \right) X = 0 \tag{19}$$

$$\dot{P} + PA - PBR^{-1} B^T P - Q + A^T P = 0 \tag{20}$$

The optimal control equation can be rewritten as

$$U^* = -R^{-1} B^T P X \tag{21}$$

The optimal control quantity U^* of the system is unrelated to the initial state of the system. In other words, regardless of the initial state of the system, the optimal control can determine the feedback control quantity by solving the feedback matrix $K = -R^{-1} B^T P$ to make the performance index of the system reach the minimum value.

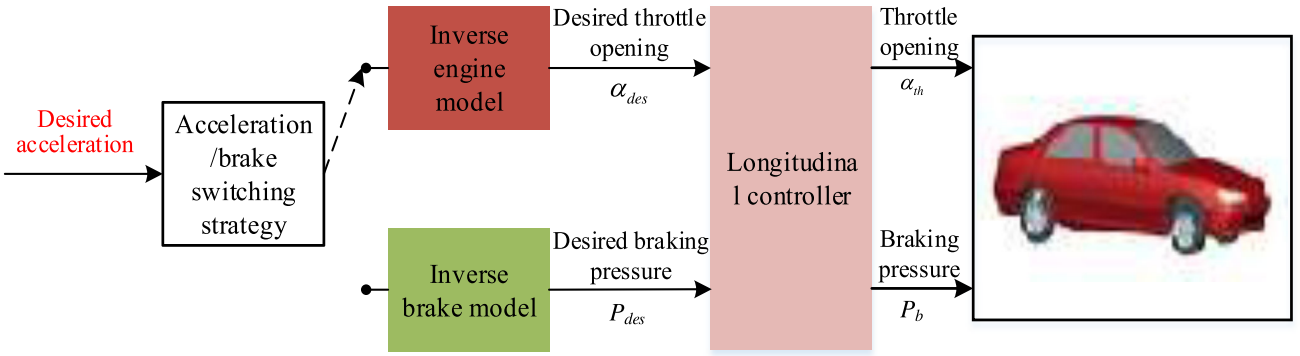

FIGURE 6. Schematic diagram of longitudinal control.

B. LONGITUDINAL CONTROLLER DESIGN

After the optimal controller is designed, the longitudinal controller is further designed. We adopt direct vertical control. The schematic is shown in Fig. 6. With the use of the longitudinal powertrain model established in Section II, an inverse engine model and an inverse brake model are established to convert the desired acceleration into a desired throttle opening and brake pressure that can be controlled.

The vehicle powertrain has strong nonlinearity. Thus, practical difficulties can be experienced when an accurate inverse engine model is being established. From (3), the output torque of the engine is a nonlinear function of the throttle opening and engine speed. Its steady-state output torque curve is shown in Fig. 7.

The look-up table module is established in MATLAB. The desired throttle opening can be obtained using the expected output torque of the engine through the offline look-up table

$$\alpha_{th} = f\left(T_{tq}, \omega\right) \tag{22}$$

Under braking conditions, when the driving force is $F_t = 0$, the relationship between the expected braking force F_x and the desired deceleration (acceleration) a_{des} can be expressed as

$$ma_{des} = -F_x - \sum F \tag{23}$$

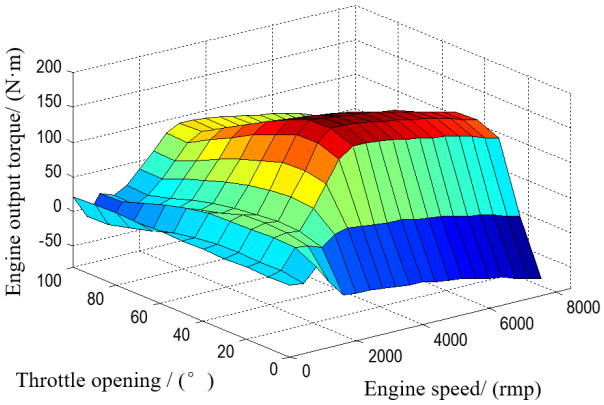

FIGURE 7. Engine static MAP chart.

Assuming that the road surface adhesion coefficient can always satisfy the braking condition, the braking force and the brake pressure of the brake cylinder can be approximated as a linear relationship as follows:

$$F_x = K_b p \tag{24}$$

where K_b is the braking coefficient.

The relationship between the desired brake pressure and the desired deceleration obtained by formulas (23) and (24)

$$Q = \begin{bmatrix} 1 & 0 & 0 & 0 \\ 0 & 1 & 0 & 0 \\ 0 & 0 & a_1 + b_1 * e^{m_1 * v} + c_1 * e^{m_1 * v} & 0 \\ 0 & 0 & 0 & a_1 + b_1 * e^{m_1 * v} + c_1 * e^{m_1 * v} \end{bmatrix};$$

$$R = \begin{bmatrix} 1 & 0 \\ 0 & a_2 + b_2 * e^{m_2 * v} + c_2 * e^{m_2 * v} \end{bmatrix}; \begin{bmatrix} a_1 \\ b_1 \\ c_1 \\ m_1 \end{bmatrix} = \begin{bmatrix} -2.77 \\ 2.65 \\ 0.57 \\ -1.1 \end{bmatrix};$$

$$\begin{bmatrix} a_2 \\ b_2 \\ c_2 \\ m_2 \end{bmatrix} = \begin{bmatrix} -1.01 \\ 0.02 \\ 13.03 \\ 0.15 \end{bmatrix};$$

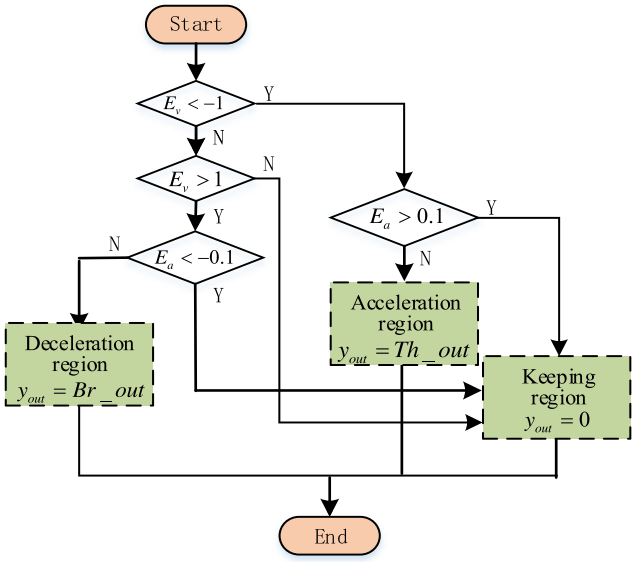

FIGURE 8. Drive / brake switching logic.

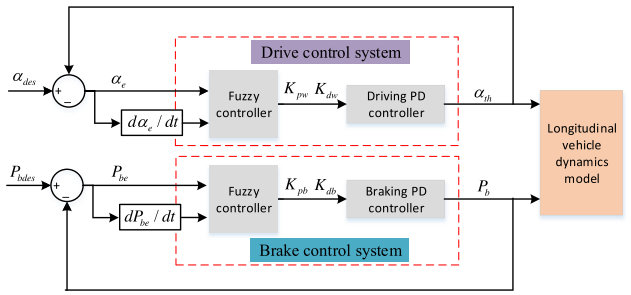

FIGURE 9. Longitudinal fuzzy PD control block diagram.

is

$$p = \frac{\left| ma_{des} + \sum F \right|}{K_b} \tag{25}$$

To ensure that the driving performance during the vehicle path tracking process meets the requirements, the following conditions should be met when the accelerator pedal and the brake pedal are working: 1) the accelerator pedal and the brake pedal cannot work at the same time; 2) and the switching between the accelerator pedal and the brake pedal should not be excessive. The logic diagram of braking and driving switching is shown in Fig. 8.

In consideration of the complex structure of the subcomponents of the vehicle powertrain and the complex nonlinear relationship, the longitudinal speed tracking controller is designed following fuzzy PD control theory. Its control block is shown in Fig. 9.

The regular expression of the PD control algorithm is

$$u(t) = k_p e(t) + k_d \frac{de(t)}{dt} \tag{26}$$

where k_p is the proportional coefficient, k_d is the differential coefficient, and $e(t)$ is the error signal.

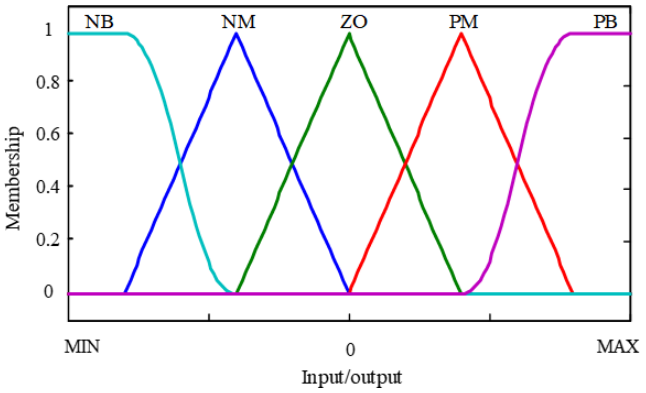

FIGURE 10. Membership function of input/output.

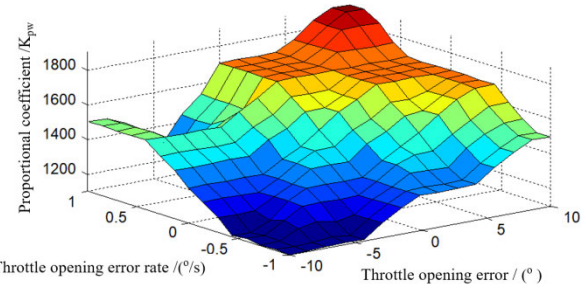

FIGURE 11. Fuzzy control regular surface of K_{pw}.

The input of the fuzzy control of the drive control system is the error value and the change rate of the desired throttle opening and the actual opening calculated by the inverse engine model. The output is the control parameters K_{pw} and K_{dw} for driving the PD controller.

The fuzzy controller mainly consists of three parts: control fuzzification, fuzzy reasoning, and deblurring. The design process is as follows:

First, the input and output variables are blurred. To consider the control effect and control difficulty, the input and output of the fuzzy controller are described by five fuzzy subsets, namely, {NB (negative big), NM (negative middle), ZO (zero), PM (positive middle), and Pb (positive big)}. The two input variables are fuzzified by using the triangle membership function trimf and the Z-type membership function zmf; the membership function of the input and output variables is shown in Fig. 10.

After obscuring the input and output variables and formulating the relevant fuzzy rules, the two output variables are deblurred by the centroid method. Figs. 11 and 12 show the fuzzy control surfaces of K_{pw} and K_{dw} after deblurring.

The design flow of the brake controller is the same as that of the drive controller. The fuzzy control surface maps of K_{pb} and K_{db} after defuzzification are shown in Figs. 13 and 14.

C. COMPENSATION CONTROLLER

During intelligent vehicle path tracking, the optimal control rate of the optimal controller planning is based on the sim-

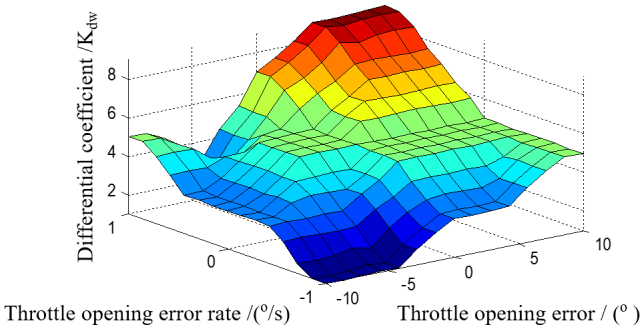

FIGURE 12. Fuzzy control regular surface of K_{dw}.

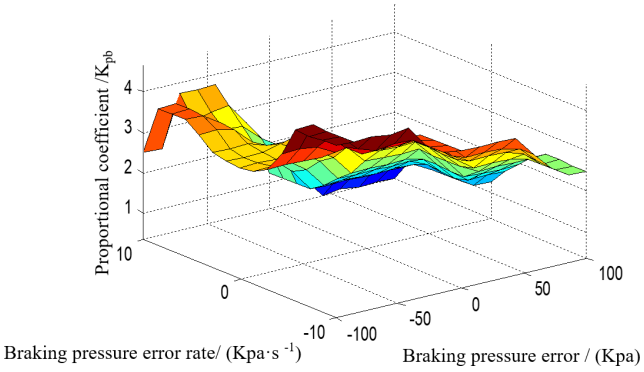

FIGURE 13. Fuzzy control regular surface of K_{pb}.

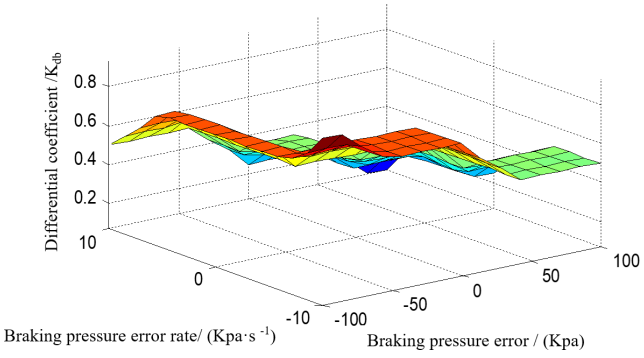

FIGURE 14. Fuzzy control regular surface of K_{db}.

plification of the vehicle model. Therefore, the error is large only through this feedforward angle control nonlinear vehicle model, which could even lead to control failure.

To ensure the accuracy of path tracking, the lateral deviation and direction deviation are initially combined into an integrated error according to a certain weight, and the integrated error and its rate of change are used as two inputs of the fuzzy controller. A reasonable fuzzy control rule is designed to output the compensation angle in real time.

The calculation rules for the integrated error are as follows:

$$E = \lambda \cdot \left[\frac{2\,(y_e - y_{\min})}{y_{\max} - y_{\min}} - 1 \right] + (1-\lambda) \cdot \left[\frac{2\,(\varepsilon_e - \varepsilon_{\min})}{\varepsilon_{\max} - \varepsilon_{\min}} - 1 \right] \tag{27}$$

TABLE 2. Vehicle main parameters.

parameter	value
Gross vehicle mass m (kg)	1495
Distance from centroid to front axle l_f (m)	1.071
Distance from centroid to rear axle l_r(m)	1.529
Inertia of vehicle rotation I_z (kg·m^2)	3053.6
Lateral stiffness of front wheel C_{af} (N·rad^{-1})	39500
Lateral stiffness of rear wheel C_{ar} (N·rad^{-1})	39500
Coefficient of road adhesion μ	0.85
rotational inertia of tires I_w (kg·m^2)	1.395
wheel radius R_w/m	0.31
Delay time of engine t_e/s	0.05
rotational inertia of engine I_e (kg·m^2)	0.19
final driver ratio R_0/-	2.87
Brake friction coefficient C_b/-	0.32

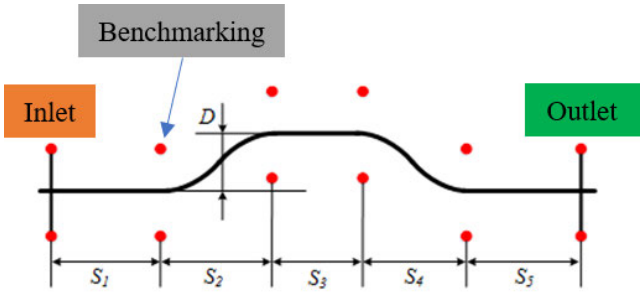

FIGURE 15. Double shift road model.

where λ is the weight coefficient, which is characterized by the degree of emphasis of the fuzzy controller on lateral deviation and direction deviation. Following Literature [**?**], we set $\lambda = 0.6$. The specific fuzzy controller derivation process is shown in Section III.B.

IV. SIMULATION VERIFICATION

To verify the effectiveness of the designed controller, the joint simulation model of the system is built in the CarSim and MATLAB/Simulink environment, and the different working conditions are simulated. The vehicle simulation parameters in the system are shown in Table 2.

A. ROAD MODEL

The road model describes the reference path of the vehicle during path tracking. The performance of the designed path tracking controller is evaluated by calculating the magnitude of the vehicle deviation during the path tracking process. To facilitate the evaluation of the designed path tracking controller, we refer to GB/T 6323-2014 standard and ISO/3888 technical report to set the double lane change (DLC) target path, as shown in Fig. 15.

The parameters of the DLC road model are shown in Table 3.

TABLE 3. Double shift path parameters.

S_1/m	S_2/m	S_3/m	S_4/m	S_5/m
65	300	25	25	65

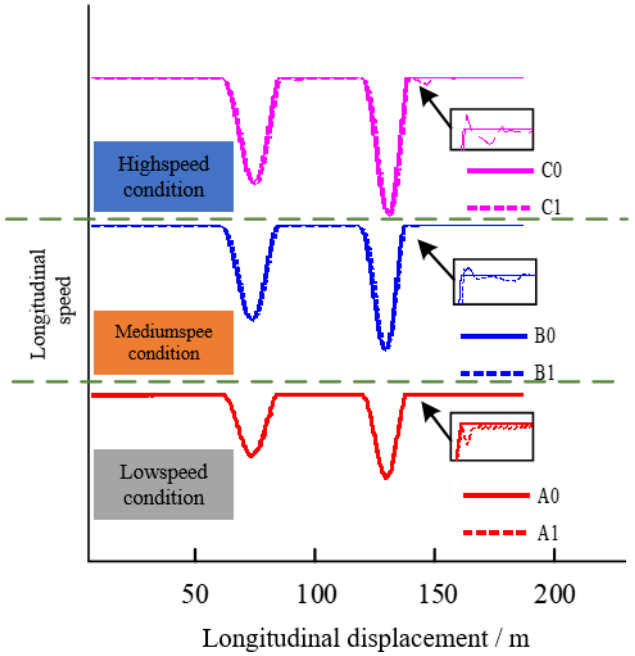

FIGURE 16. Longitudinal speed.

TABLE 4. Simulink results.

	A	B	C
Longitudinal acceleration.	1.718232	2.58011	2.872928
Lateral error	0.049763	0.063981	0.110427
Deviation in direction	4.600462	5.431871	5.524249

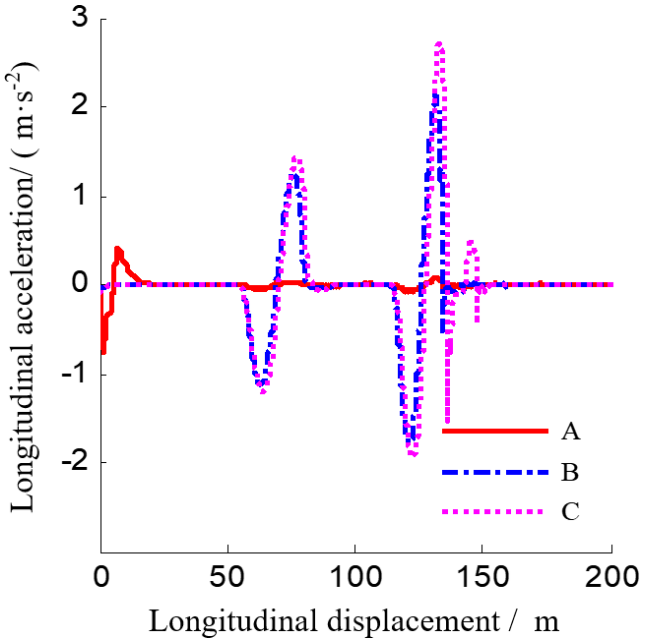

FIGURE 17. Longitudinal acceleration.

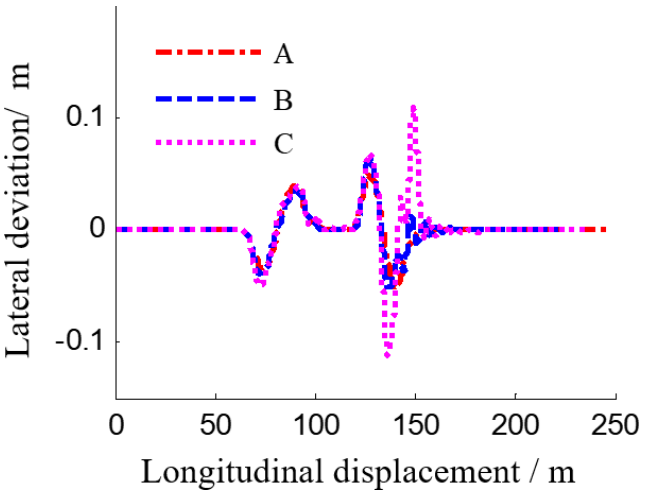

FIGURE 18. Lateral error.

B. COMPARATIVE ANALYSIS OF DIFFERENT INITIAL VEHICLE SPEEDS

Simulation analysis is conducted at initial speeds of 5, 15, and 20 m/s respectively, and the adhesion coefficient is set as $\mu = 0.85$. In this manner, the designed hierarchical path tracking control system is verified to track the path along the planned speed of the upper optimal controller at different initial speeds. The results are shown from Figure 16 to Figure 19, and the peak values of A, B and C are shown in Table 4.

Figs. 16 and 17 show the vehicle speed tracking diagram and longitudinal acceleration comparison diagram of the longitudinal control system under three vehicle speeds, respectively. A, B, and C are the speed tracking graphs of three different speeds, respectively. The peak values of longitudinal acceleration for A, B and C are 1.718232, 2.58011 and 2.872928 m/s^2 respectively, which implies that the designed longitudinal and lateral coordinated control system can tracking of different expected speeds during vehicle path tracking.

Figs. 18 and 19 show the effect diagrams of tracking the DLC path under three vehicle speeds and the comparison of lateral deviation and direction deviation, respectively. The designed longitudinal and lateral coordinated controller can both track the expected speed and path stably, and the tracking error is within a reasonable range based on the results of Table 5.

C. DIFFERENT ROAD ENVIRONMENTS

To verify whether the vehicle has good path tracking ability on different road surfaces, taking the initial speed of 15 m/s as an example, the simulation analysis is conducted on the

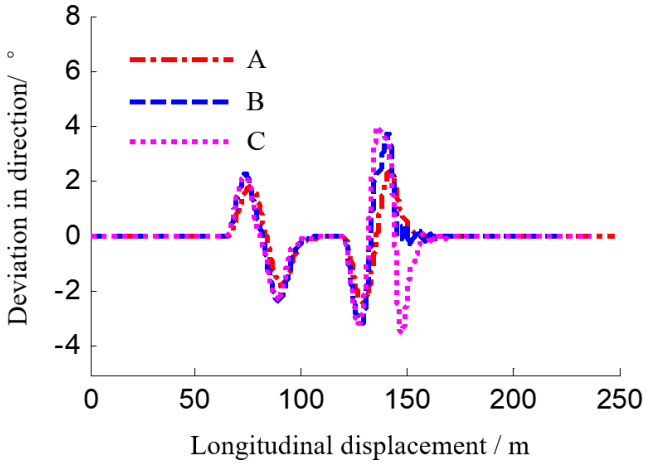

FIGURE 19. Deviation direction.

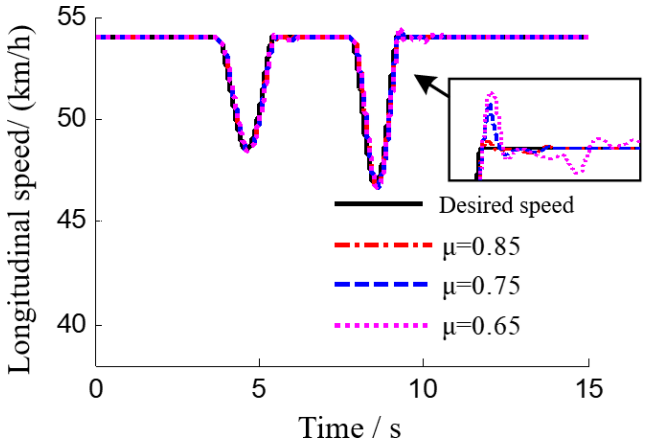

FIGURE 20. Longitudinal speed.

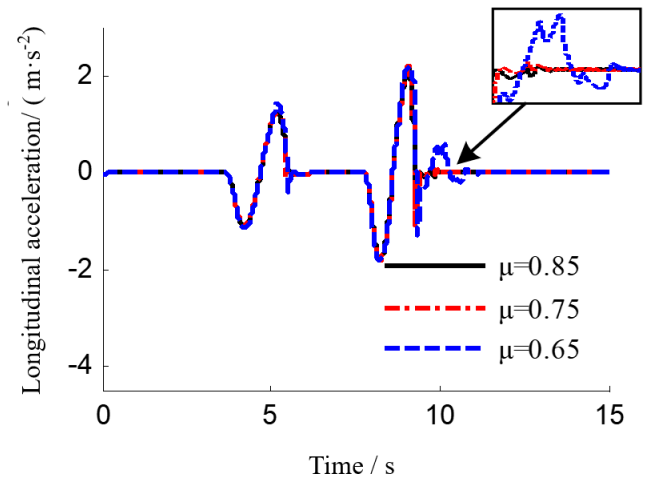

FIGURE 21. Longitudinal acceleration.

road with adhesion coefficient of $\mu = 0.85$, $\mu = 0.75$, and $\mu = 0.65$. The simulation results are shown from Figs. 20 to Fig 24, and the peak values under three road surfaces with different adhesion coefficient are shown in Table 5.

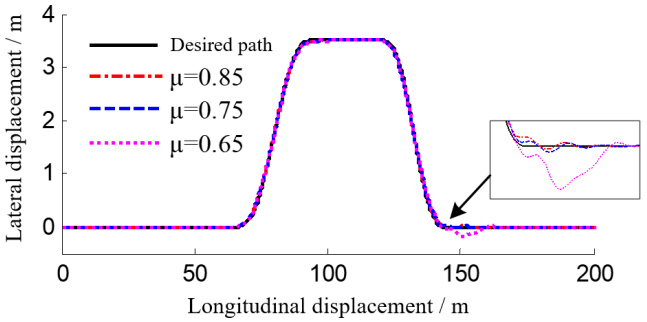

FIGURE 22. Longitudinal acceleration.

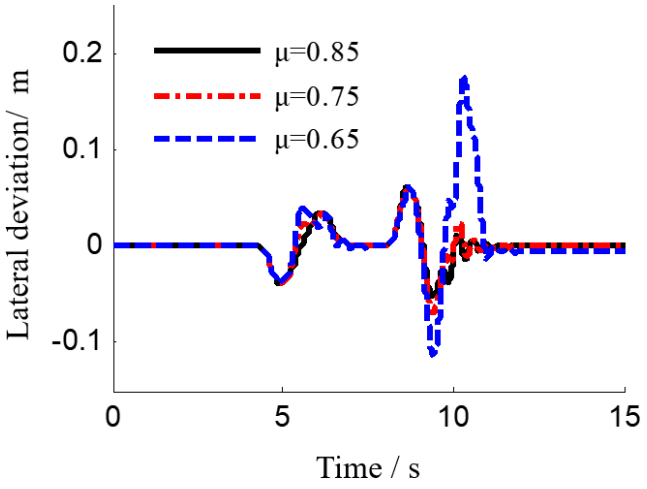

FIGURE 23. Lateral error.

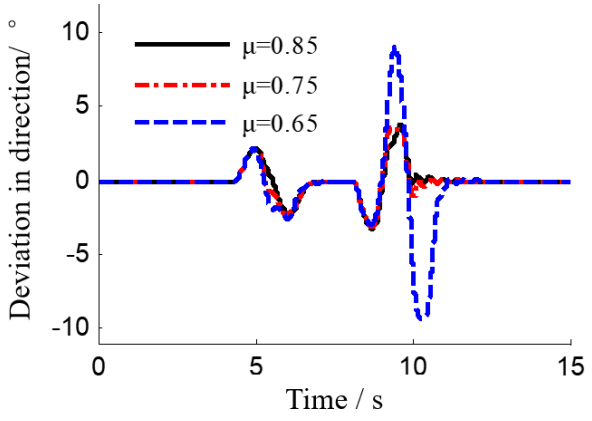

FIGURE 24. Directional error.

Figs. 20 and 21 show the time-domain response diagrams of longitudinal velocity and acceleration on different roads at an initial speed of 15 m/s. As shown in the figures, the vehicle tracks the desired speed in different road environments stably, and the longitudinal acceleration does not exceed 3 m/s^2. As shown in Table 5, the peak values of longitudinal acceleration under three different road surfaces are 2.1429, 2.1754 and 2.1922 m/s^2 respectively, thus indicating good longitudinal performance.

TABLE 5. Simulink results.

	μ=0.85	μ=0.75	μ=0.65
Longitudinal acceleration	2.1429	2.1754	2.1922
Lateral error	0.0617	0.0609	0.1782
Deviation in direction	3.7275	3.6465	9.0553

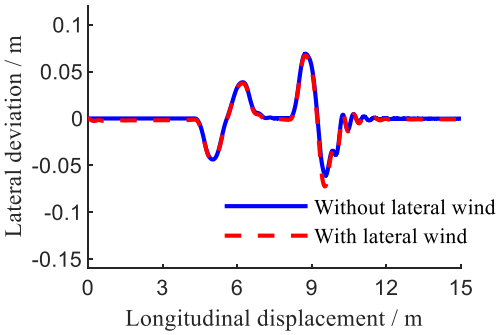

FIGURE 25. Lateral deviation comparison.

TABLE 6. Simulink results.

	With lateral wind	Without lateral wind
Lateral deviation	0.070881	0.06875
Deviation in direction	3.6706	3.6346

Figs. 22–24 show the DLC tracking diagrams of the vehicle on three different road surfaces at the initial vehicle speed of 15 m/s as well as the comparison of lateral deviation and direction deviation. The simulation diagram shows that, in different road environments, the vehicle, which has good path tracking ability, tracks the desired path stably. The peak values of lateral error and deviation in direction of the vehicle under three different road surfaces are shown in Table 5, and they both are controlled within a reasonable range.

D. ROBUSTNESS ANALYSIS

A complete path tracking system should have good anti-disturbance capability and strong robustness. This section verifies the robustness of the proposed path tracking system by adding lateral wind disturbances and changing the sprung mass during the co-simulation process. The initial simulation speed is set to 54 km/h.

Lateral wind is a common nonlinear disturbance during vehicle driving, and it occurs particularly at high-speed driving and affects vehicle tracking accuracy and steering stability. To test the nonlinear interference capability of the designed path tracking control system, a 50 km/h lateral wind model is added in the CarSim simulation condition. The results are shown from Figs. 25 to Fig 28, and they peak values are shown in Table 6.

It can be seen that under the action of the lateral wind, the peak value of the lateral deviation and the direction deviation only has a little increase compared with that of the non-lateral wind, that is, the designed fuzzy compensation controller is robust to lateral wind disturbance. In addition, 200 and 350 kg are loaded on the basis of the original sprung mass. The change in the position of the center of mass caused by the increase in the sprung mass is ignored. Furthermore, in comparing with sprung mass change of Figs.27 and 28, the change of lateral deviation is less than 0.03m, the change of direction deviation is less than 0.2 °, and the time-domain response curve is basically consistent. Therefore, the designed longitudinal and lateral coordinated controller can offset the influence of nonlinear and parameter changes in the vehicle driving process to a certain extent and has good robustness.

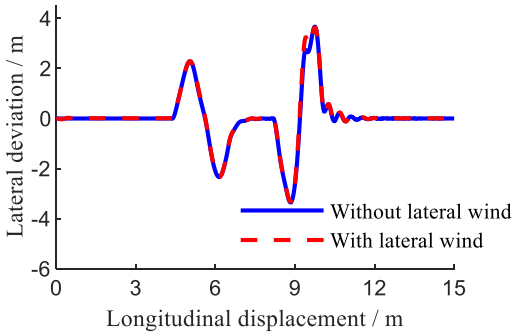

FIGURE 26. Directional in deviation comparison.

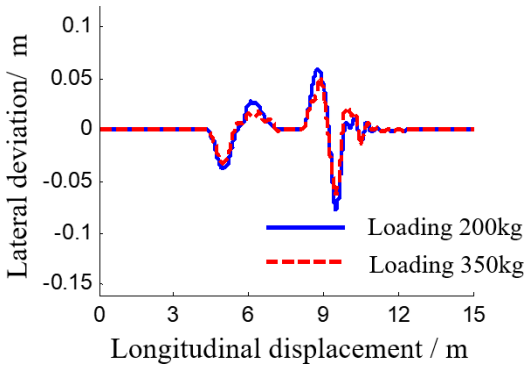

FIGURE 27. Comparison of lateral error.

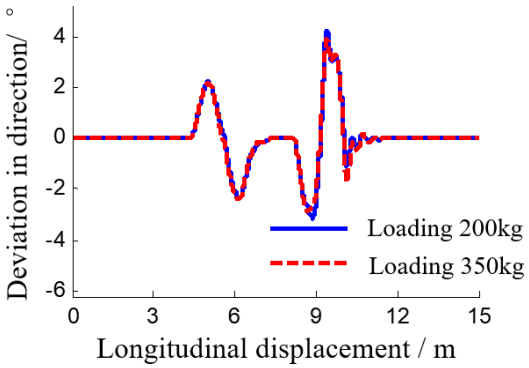

FIGURE 28. Comparison of direction error.

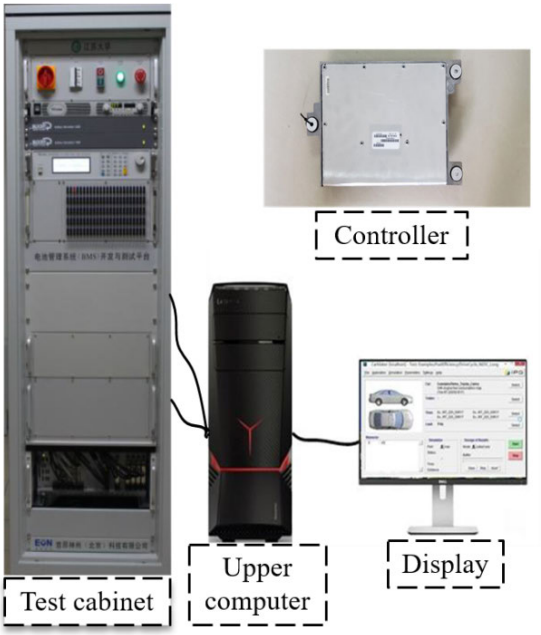

FIGURE 29. Block diagram of HCU HiL system.

TABLE 7. Longitudinal acceleration.

	Co-simulation	HiL test
Initial speed:18km/h	0.29913	0.309565
Initial speed:72km/h	2.49741	2.74611

V. TEST VERIFICATION

To verify the feasibility of the control system design, we redevelop the HIL simulation test platform. On the basis of the rapid control prototype, the control algorithm is compiled into executable code and downloaded to the controller to verify the operational efficiency of the control algorithm. The HIL test platform is shown in Fig. 29.

A. VARIABLE SPEED CONDITION

First, in order to verify the performance of the longitudinal control system, the optimal speed planned by the optimal controller under the initial vehicle speed of 18 km/h and 72 km/h are separately taking as the tracking target and the time-domain response of the longitudinal performance under two different conditions are shown in FIGURE.30 to 31.

From FIGURE 30 to 31, it can be seen that the designed longitudinal control system can stably track the expected vehicle speed under the condition which can satisfy the requirements of road adhesion. Furthermore, the longitudinal acceleration is always less than 3 m/s^2, which is enough to meet the requirements of driving conditions.

B. DLC ROAD

To verify the path tracking capability of the longitudinal and lateral coordinated control system, an initial speed tracking of 54 km/h is used as an example. Fig. 32 shows the HiL test and pure simulation tracking during the situation where the longitudinal speed can stably track the optimal speed.

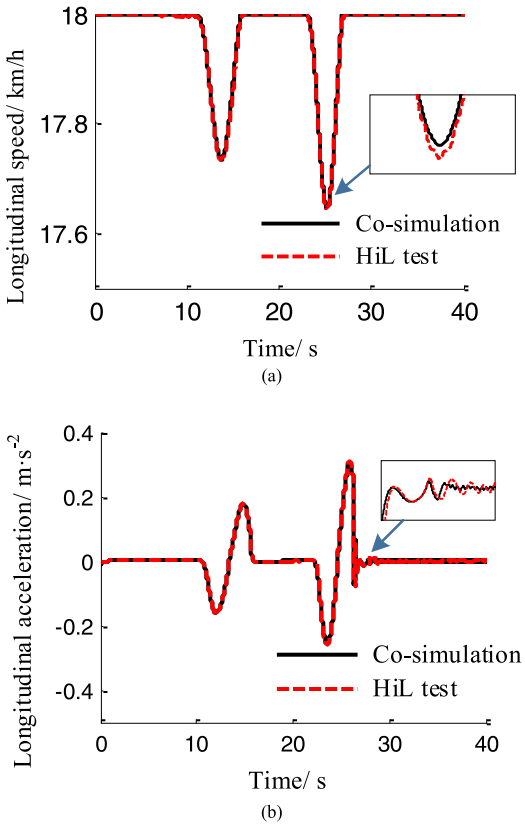

FIGURE 30. Initial speed: 18km/h. (a) Tracking of longitudinal speed; (b) Time-domain response of longitudinal acceleration.

TABLE 8. Simulink results.

	Co-simulation	HiL test
Lateral deviation	0.062857	0.077143
Deviation in direction	3.69863	8.57534

The effect diagrams of the double shifting line as well as the tracking performance and driving performance indicators of the vehicle during the tracking are shown in Figs. 33 and 34. Meanwhile, the peak values of lateral deviation and deviation in direction on Co-simulation and HiL test are shown in Table 7.

As shown in Table 8, the peak value of the lateral deviation between Co-simulation and HiL test only has a little increase. As for deviation in direction, it's very close between the two except at the peak. But as you can see from Figs. 33 and 34, there is a fluctuation on HiL-test at about 10 s, which is caused by an accidental test error. Therefore, the longitudinal and lateral coordinated control system has a good path tracking capability.

C. SMOOTHLY CURVED ROADS

To verify the stability of the path tracking system on smoothly curved roads, the results of the HIL test are compared with the pure simulation results. Fig. 35 shows the comparison of

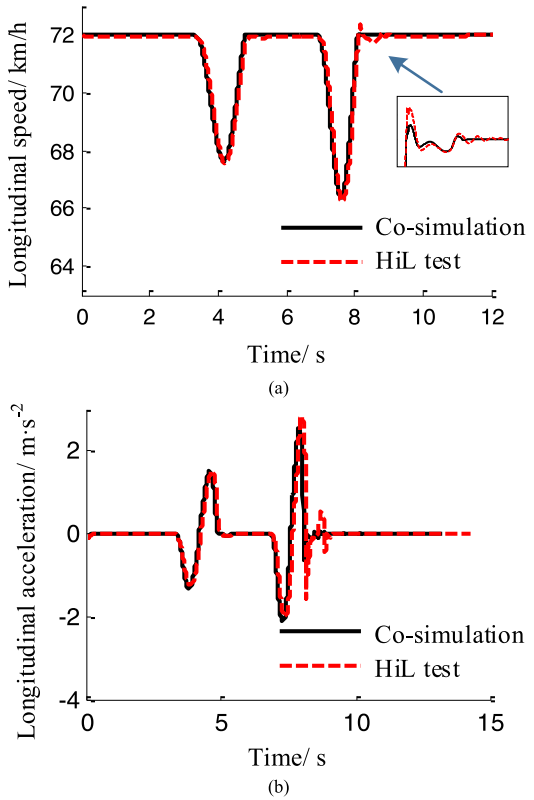

FIGURE 31. Initial speed: 72km/h. (a) Tracking of longitudinal speed; (b) Time-domain response of longitudinal acceleration.

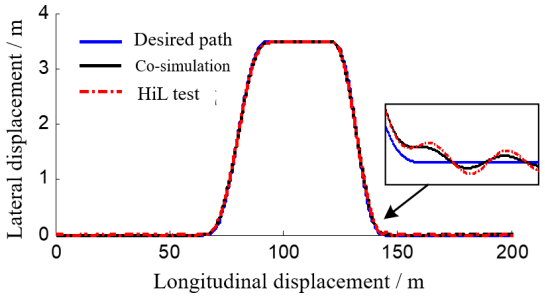

FIGURE 32. Double line path tracking.

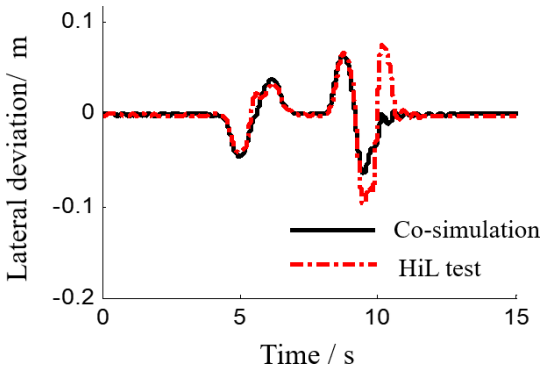

FIGURE 33. Comparison of lateral error.

tracking results obtained by HIL and pure simulation as the vehicle drives along a smooth curve. Figs. 36 and 37 show the comparison of longitudinal driving performance, path

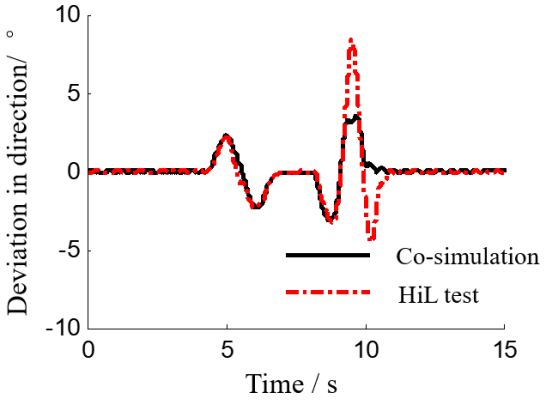

FIGURE 34. Comparison of deviation in direction.

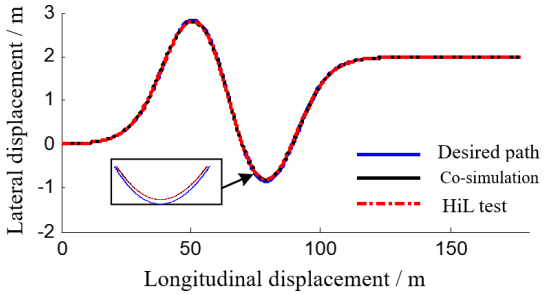

FIGURE 35. Smooth curve tracking.

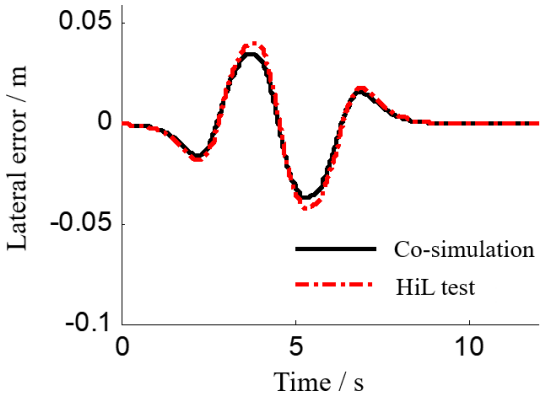

FIGURE 36. Comparison of lateral error.

tracking performance, and steering performance during the tracking process.

The simulation diagram shows that, compared with the CarSim/Simulink joint simulation, the time-domain response curve of HIL test is basically consistent, and the online simulation accuracy is slightly poor primarily due to the small-time delay and nonlinear interference of the controller. In sum, the HIL simulation results show that the real-time performance and the effectiveness of the designed longitudinal and lateral coordinated path tracking controller meet the requirements. Therefore, the designed longitudinal and lateral coordinated controller is effective in real environments.

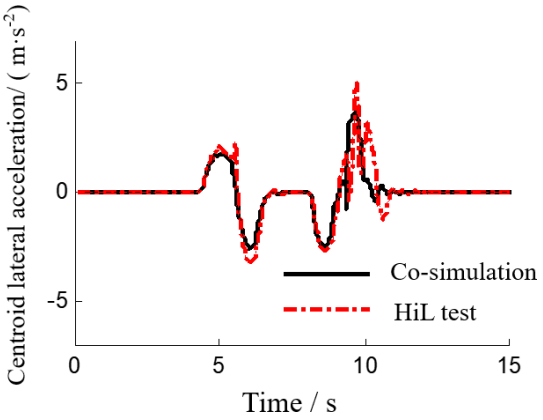

FIGURE 37. Centroid lateral acceleration.

VI. CONCLUSION

In this paper, the high nonlinearity and complex longitudinal-lateral coupling relationship of the proposed system during intelligent vehicle path tracking is studied. And based on which, a new intelligent vehicle longitudinal and lateral coordinated control algorithm is proposed. To this end, a nonlinear dynamics model, a tire model, and a vehicle powertrain model including longitudinal and lateral coupling are constructed. The longitudinal and lateral coordinated control system of the intelligent vehicle is designed, in which the upper controller is the optimal controller that can plan the optimal vehicle speed and the optimal front wheel angle in real time, and the lower controller is the lateral fuzzy controller with steering angle compensation to improve the accuracy of the path tracking. On this basis, the vehicle speed tracking controller is designed and the longitudinal and lateral coordinated control of the vehicle is realized. Finally, the effectiveness of the designed longitudinal and lateral coordinated path tracking control algorithm is verified by CarSim/Simulink joint simulation and HIL test. The results show that the designed hierarchical path tracking control system can predict the expected vehicle speed in real time at different initial speeds, control the vehicle's adaptive acceleration and deceleration to achieve path tracking, and balance the tracking performance and driving performance under different vehicle speeds, so as that the dynamic optimization of tracking performance and driving performance during vehicle path tracking is guaranteed. Further study on effect of road condition in IV path tracking system will be conducted in the near future.

REFERENCES

[1] M. Welde and J. Odeck, "Evaluating the economic impacts of intelligent transport systems," in *Proc. 14th World Congr. Intell. Transp. Syst.*, Beijing, China, Oct. 2007.
[2] Z. Liang, J. Zhao, Z. Dong, "Torque vectoring and rear-wheel-steering control for vehicle's uncertain slips on soft and slope Terrain using sliding mode algorithm," *IEEE Trans. Veh. Technol.*, vol. 69, no. 4, pp. 3805–3815, Apr. 2020.
[3] J. Ziegler, "Making bertha Drive—An autonomous journey on a historic route," *IEEE Intell. Transp. Syst. Mag.*, vol. 6, no. 2, pp. 8–20, Apr. 2014.
[4] J. Ploeg, E. Semsar-Kazerooni, G. Lijster, N. van de Wouw, and H. Nijmeijer, "Graceful degradation of cooperative adaptive cruise control," *IEEE Trans. Intell. Transp. Syst.*, vol. 16, no. 1, pp. 488–497, Feb. 2015.
[5] Y. Xia, F. Pu, S. Li, and Y. Gao, "Lateral path tracking control of autonomous land vehicle based on ADRC and differential flatness," *IEEE Trans. Ind. Electron.*, vol. 63, no. 5, pp. 3091–3099, May 2016.
[6] W. Li, Z. Xie, P. K. Wong, "Adaptive-event-triggered-based fuzzy nonlinear lateral dynamic control for autonomous electric vehicles under insecure communication networks," *IEEE Trans. Ind. Electron.*, early access, Feb. 7, 2020, doi: 10.1109/TIE.2020.2970680.
[7] K. Lee, S. Jeon, H. Kim, and D. Kum, "Optimal path tracking control of autonomous vehicle: Adaptive full-state linear quadratic Gaussian (LQG) control," *IEEE Access*, vol. 7, pp. 109120–109133, 2019.
[8] C. Sun, X. Zhang, Q. Zhou, and Y. Tian, "A model predictive controller with switched tracking error for autonomous vehicle path tracking," *IEEE Access*, vol. 7, pp. 53103–53114, 2019.
[9] R. Marino, S. Scalzi, G. Orlando, and M. Netto, "A nested PID steering control for lane keeping in vision based autonomous vehicles," in *Proc. Amer. Control Conf.*, 2009, pp. 2885–2890.
[10] A. Goodarzi, A. Sabooteh, and E. Esmailzadeh, "Automatic path control based on integrated steering and external yaw-moment control," *Proc. Inst. Mech. Eng. K, J. Multi-Body Dyn.*, vol. 222, no. 2, pp. 189–200, Jun. 2008.
[11] J. Huang and M. Tomizuka, "LTV controller design for vehicle lateral control under fault in rear sensors," *IEEE/ASME Trans. Mechatronics*, vol. 10, no. 1, pp. 1–7, Feb. 2005.
[12] J. Duan, J. Yao, D. Liu, and G. Liu, "A path tracking control algorithm with speed adjustment for intelligent vehicle," in *Proc. IEEE Int. Conf. Robot. Biomimetics (ROBIO)*, Dec. 2013, pp. 2397–2402.
[13] C. Gámez Serna and Y. Ruichek, "Dynamic speed adaptation for path tracking based on curvature information and speed limits," *Sensors*, vol. 17, no. 6, p. 1383, 2017.
[14] L. F.-Y. L. Wang, and E. Boston, "Advanced vehicle longitudinal motion control," in *Advanced Motion Control and Sensing for Intelligent Vehicles*. Boston, MA, USA: Springer, 2007, pp. 135–184.
[15] S. H. HosseinNia, I. Tejado, B. M. Vinagre, V. Milanes, and J. Villagra, "Low speed control of an autonomous vehicle using a hybrid fractional order controller," in *Proc. 2nd Int. Conf. Control, Instrum. Autom.*, Dec. 2011, pp. 116–121.
[16] J. Maojing, "Improvement of road-following intelligent speed control based on road curvature," in *Proc. 3rd Int. Conf. Intell. Syst. Design Eng. Appl.*, Jan. 2013, pp. 870–873.
[17] Z. Fang, J. Duan, and B. Zheng, "Longitudinal motion control of intelligent vehicle based on two hierarchies optimal method," in *Proc. Chin. Autom. Congr. (CAC)*, Nov. 2015, pp. 1092–1097.
[18] K. El Majdoub, F. Giri, H. Ouadi, L. Dugard, and F. Z. Chaoui, "Vehicle longitudinal motion modeling for nonlinear control," *Control Eng. Pract.*, vol. 20, no. 1, pp. 69–81, Jan. 2012.
[19] W. T. Kirchner and S. C. Southward, "Adaptive vehicle traction control: Combined longitudinal and lateral motion," *Int. J. Dyn. Control*, vol. 1, no. 3, pp. 239–253, Sep. 2013.
[20] L. Li, F. Y. Wang, and Q. Zhou, "Integrated longitudinal and lateral Tire/Road friction modeling and monitoring for vehicle motion control," *IEEE Trans. Intell. Transp. Syst.*, vol. 7, no. 1, pp. 1–19, Mar. 2006.
[21] Li, Jia, Cheng, "Optimal model predictive control for path tracking of autonomous vehicle," in *Proc. 3rd Int. Conf. Meas. Technol. Mechatronics Automat.*, Jan. 2011, pp. 791–794.
[22] L. Menhour, B. D'Andrea-novel, M. Fliess, and H. Mounier, "Multivariable decoupled longitudinal and lateral vehicle control: A model-free design," in *Proc. 52nd IEEE Conf. Decis. Control*, Dec. 2013, pp. 2834–2839.
[23] S. Kumarawadu and T. T. Lee, "Neuroadaptive combined lateral and longitudinal control of highway vehicles using RBF networks," *IEEE Trans. Intell. Transp. Syst.*, vol. 7, no. 4, pp. 500–512, Dec. 2006.
[24] L. Chunfu, C. Huiyan, and T. Gang, "Arithmetic of the cooperating point of engine and torque converter," *Trans. Chin. Soc. Agricult. Mach.*, vol. 40, no. 3, pp. 11–15, 2009.
[25] Q. Ye, R. Wang, Y. Cai, X. Xu, X. Meng, and C. Long, "A study of the novel vision guided IV trajectory tracking control system based on expected yaw velocity," *Adv. Eng. Softw.*, vol. 131, pp. 196–204, May 2019.

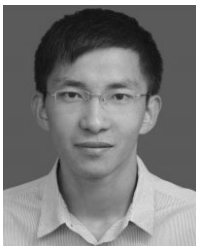

ZEYUN SUN received the B.S. and M.S. degrees in vehicle engineering from Jiangsu University, Zhenjiang, Jiangsu, China, in 2010 and 2013, respectively, where he is currently pursuing the Ph.D. degree in vehicle engineering.

His research interests include vehicle dynamic, coordinated control, intelligent vehicle path tracking control, vehicle suspension dynamic, and steering system dynamic.

RUOCHEN WANG received the B.S. degree in mechanical engineering from Luoyang Polytechnic, Luoyang, Henan, China, in 2001, and the Ph.D. degree in vehicle engineering from Jiangsu University, Zhenjiang, Jiangsu, China, in 2006.

From 2006 to 2009, he was a Lecturer and from 2009 to 2014, he was an Associate Professor. Since July 2014, he was a Professor with the School of Automotive and Traffic Engineering, Jiangsu University. His research interests include vehicle dynamic performance simulation and control, intelligent vehicle systems, new energy vehicle, and electricity generation system of automobile exhaust temperature difference.

QING YE received the M.Eng. degree and the Ph.D. degree with dynamic research of intelligent vehicle from the School of Automatic and Traffic Engineering, Jiangsu University, Jiangsu, China, in 2012 and 2019, respectively.

He has authored over ten articles and received ten patents. His research interests include vehicle dynamic, coordinated control, intelligent vehicle path tracking control, vehicle suspension dynamic, time delay mechanism, and steering system dynamic.

ZHENDONG WEI received the B.S. and M.S. degrees in vehicle engineering from Jiangsu University, Zhenjiang, Jiangsu, China, in 2016 and 2019, respectively.

He is currently working on intelligent vehicle path tracking control. His research interests include vehicle dynamic, coordinated control, intelligent vehicle path tracking control, vehicle suspension dynamic, and steering system dynamic.

BINGQING YAN received the B.S. and M.S. degrees in vehicle engineering from Jiangsu University, Zhenjiang, Jiangsu, China, in 2016 and 2019, respectively.

He is currently working on intelligent vehicle path tracking control. His research interests include vehicle dynamic, coordinated control, intelligent vehicle path tracking control, vehicle suspension dynamic, and steering system dynamic.